IEEE Access
Multidisciplinary | Rapid Review | Open Access Journal

Received December 16, 2021, accepted January 4, 2022, date of publication January 7, 2022, date of current version January 13, 2022.

Digital Object Identifier 10.1109/ACCESS.2022.3141421

A Total-Cross-Tied-Based Dynamic Photovoltaic Array Reconfiguration for Water Pumping System

GADIRAJU HARISH KUMAR VARMA, (Graduate Student Member, IEEE), VENUGOPAL REDDY BARRY, (Member, IEEE), AND ROHIT KUMAR JAIN
Department of Electrical and Electronics Engineering, National Institute of Technology Goa, Ponda, Goa 403401, India

Corresponding author: Gadiraju Harish Kumar Varma (gadiraju.harish@gmail.com)

This work was supported by the Science and Engineering Research Board (SERB), Department of Science and Technology, Government of India, through the Research Project titled "Design and Development of a Dynamic Photovoltaic Array fed Single-Stage PV Pumping System Using an Open-End Winding Induction Motor," under Grant CRG/2018/003908.

ABSTRACT Most Photo-voltaic (PV) applications require a shadow-free area for the installation of the PV panels. However, shading is inevitable in a few applications like building-integrated PV pumping systems (BIPVPS). Partial shading occurs due to soiling, clouds, shades of nearby trees, buildings, current, and telephone poles. During this partial shading condition, the PV array output power decreases, reducing the efficiency of the BIPVPS. In this paper, a novel dynamic array reconfiguration technique is proposed to enhance the power output from the PV array. The proposed system uses a boost converter with an incremental conductance algorithm for operating enhanced power at the maximum. Sinusoidal Pulse Width Modulation (SPWM) technique based on V/f control operates the induction motor. Thus, the proposed algorithm and maximum power point technique (MPPT) enhance the power output from the PV array and track the global power. The PI and V/f control regulate the dc-link voltage and speed of the Induction motor. Simulations and experimental studies are performed to show the effectiveness of the proposed algorithm. The proposed system results in additional 234 W PV power extraction compared to the conventional system. Thus, making the proposed BIPVPS efficient.

INDEX TERMS Partial shading, dynamic reconfiguration, total-cross-tied, power enhancement, PV water pumping.

I. INTRODUCTION

Photovoltaic (PV) based energy generation technologies have been at the forefront among renewables for power generation. Building-integrated photovoltaic pumping systems (BIPVPS) have gained increasing interest as a PV technology application over the last few decades [1]. Unlike conventional water pumps, correctly designed and sized PV water pumps can provide long-term savings.

A wide range of research has been done on PV water pumping systems [2]. It includes improving photovoltaic arrays efficiency, electric motor and pumps interaction against the irradiance variation, designing the motors for specific water pumping applications, and various maximum power point techniques (MPPT) [3]. Further, research also involves cost reduction, productivity gain, and life expansion of PV water pumping systems. However, there is scope to examine the PV water pumping system performance under partial shading conditions (PSC). It has a significant effect on the BIPVPS because of the poles and shading of the nearest buildings.

Partial shading conditions reduce the output power from the PV array [4]. In literature to revamp this issue primarily uses a bypass diode. Although these diodes protect the PV panel from the hot spot effect, they result in multiple peaks [5]. These multiple peaks make the conventional MPPT converge at the local maximum. Several artificial intelligence and bio-inspired algorithms are applied to overcome the ineffectiveness to track the maximum global power under partial shading conditions [6]. However, the global maximum power point techniques (GMPPT) cannot effectively utilize the PV array to enhance the maximum power.

The second category includes different PV array topologies. They reduce the mismatch losses during PSC [7]. The PV water pumping system commonly uses the series-parallel arrangement [8], [9]. However, Total-Cross-Tied (TCT) topology has better performance during most of the shading

The associate editor coordinating the review of this manuscript and approving it for publication was Chi-Seng Lam.

conditions [10]. So, this paper uses TCT topology for the proposed system. Distributed MPPT (DMPPT) also improves the PV array performance during PSC but requires more converters, thus making the PV water pumping system expensive [11].

Finally, reconfiguration provides a feasible solution to mitigate this problem. For a higher size PV array, static reconfiguration is economical as it does not require irradiance sensors and switches [12]. On the other hand, the BIPVPS system requires a lower-size PV array, making dynamic photovoltaic array reconfiguration (DPVAR) attractive for this application. The inherent advantage of the DPVAR is that it is applied to any shading condition [13]. Moreover, dynamic reconfiguration (DR) enhances the power to the maximum possible extent compared to all the mitigation approaches [14].

Over the past few years various PV water pumping systems are developed [15]–[23]. The different motors used for this application are elaborated in the literature [2]. The Induction motor is a wise choice for this application due to enormous advantages [8], [22], [23]. The induction motor design methodology was investigated extensively for improving the efficiency of the system [25], [26]. Although the design of the motor improves the efficiency, the effective utilization of PV array during partial shading has a significant effect on the overall efficiency of the PV water pumping system [26]. Therefore, in the proposed method to improve the overall system efficiency, emphasis is made on extracting and enhancing the maximum power from the PV array using an conventional induction motor.

Induction motor-based pumping is classified as single-stage and two-stage. The single-stage topology of the solar PV array system does not require a boost converter. However, both the benefits of MPPT and dc-link voltage control are achieved through the inverter. In two-stage, the primary stage comprises a boost converter, and the second stage is an inverter used for motor control [8]. However, most of the studies above assume uniform shading over the PV array and have done minimal research on partial shading conditions [23], [24], [28].

In [23], the effects of partial shading on series-parallel topology for PV water pumping system is elaborated. It is observed that the global peak location on the left side of the P-V curve during partial shading significantly affects the DC-DC converter operation. The maximum PV array voltage will be less during these cases. So the boost converter should operate at a higher duty ratio to meet the required dc-link voltage. A higher duty ratio will lead to higher switching stress and lower efficiency. A single-ended primary inductor converter (SEPIC) based on multi-input single-output (SEPIC-MISO) is used for photovoltaic water pumping system in [31] to reduce the stress on the circuit components and to improve the system's reliability. In paper [32], reconfiguration for PV water pumping system is developed, where the algorithm verifies all the combinations of irradiances to generate the maximum output power. Further, in [33], a cuckoo search algorithm is used for tracking global peak under partial shading conditions. However, it does not enhance the output power from the PV array under partial shading conditions.

This paper proposed a novel dynamic array reconfiguration method to solve the above-mentioned problems. In the proposed method, the peak always occurs on the right side of the $P-V$ curve, maintaining the peak voltage almost constant similar to uniform shading conditions, thus reducing the burden on the DC-DC converter. The proposed method used a TCT PV array for reconfiguration. The MPPT algorithm extracts the maximum energy from the PV array using a boost converter. The PI controller regulates the dc-link voltage. The inverter controller controls the motor speed according to PV irradiance operating at the MPP.

A. CONTRIBUTIONS & ORGANIZATION OF THE PAPER

The main contributions of this paper are as follows:

1. Most of the research on PV water pumping system focus on uniform shading conditions applied on series-parallel topology. However, this paper uses TCT topology for improving the performance of BIPVPS under partial shading conditions.
2. This paper proposes a novel dynamic reconfiguration (DR) for TCT topology using irradiance sensors for power enhancement to improve the water discharge at any shading conditions.
3. The proposed algorithm avoids the necessity of complex optimization algorithms for tracking MPP even under partial shading conditions.

The rest of this paper organizes as follows: Section II describes the modelling and design analysis. Section III presents the control scheme. Section IV analyzes the simulation and experimental results. Finally, Section V ends with a conclusion.

The following nomenclature is used in the rest of the paper.

Nomenclature:

η_d	Efficiency of motor drive.
η_p	Efficiency of the pump.
ω	Reference speed.
ω_1	Speed corresponding to PI controller.
ω_2	Speed corresponding to PV power.
ρ	Specific gravity of water.
C_{dc}	Dc-link capacitance.
C_{PV}	Boost converter capacitance.
f_s	Switching frequency.
G	Irradiance matrix.
H	Total head.
I_{mp}	Current at maximum power.
I_{PV}	PV array current.
I_{sc}	Short circuit current.
I_S	Number of irradiance sensors.
L	Boost converter inductance.
m	Number of rows.

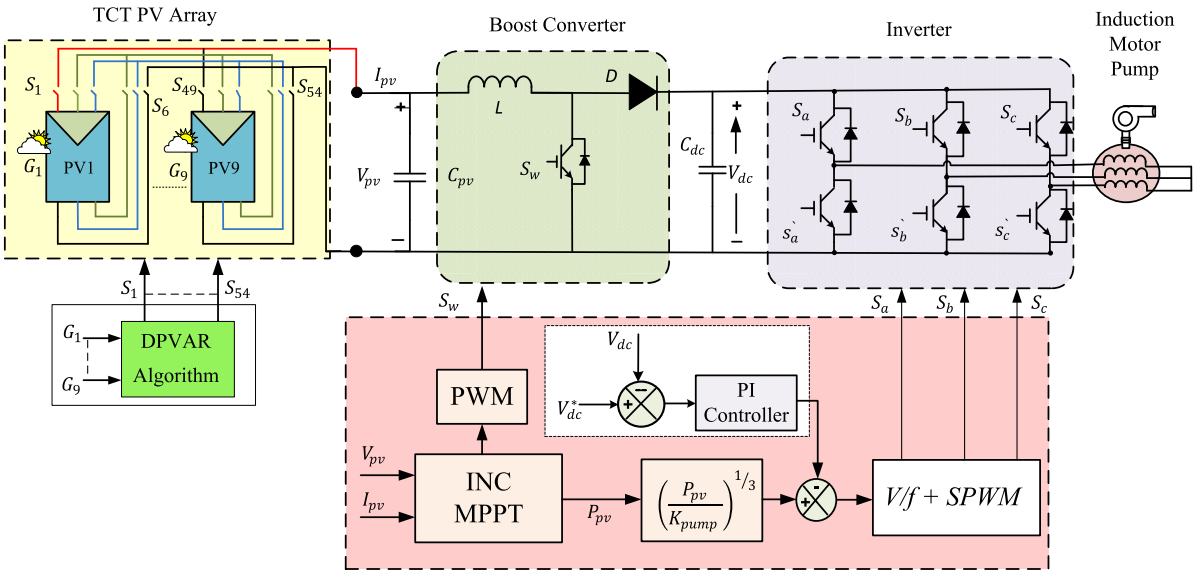

FIGURE 1. Block diagram of TCT based PV water pumping system.

m_a	Modulation index.
N	Number of PV modules.
n	Number of columns.
P	Position matrix.
P_{mp}	Maximum power of a PV module.
P_{PV}	PV array power.
Q	Flow discharge.
t	Transient duration.
T_L	Load torque.
V_{dc*}	Reference dc-link voltage.
V_{dc_1}	Lower most dc-link voltage during transient.
V_{dc}	Dc-link voltage.
V_{LL}	Motor voltage.
V_{mp}	Voltage at maximum power.
V_{oc}	Open circuit voltage.
V_{PV}	PV array voltage.

II. MODELLING & DESIGN PROCESS

Fig. 1 shows the block diagram of the proposed system. The sizing of the system starts with a correct estimation of load (water requirement). The motor design depends on the load requirement. Later, the TCT PV array is modelled for the required motor rating. The proposed algorithm requires switches, sensors, and controllers for its operation. The following section elaborates the design of all these components:

A. DESIGN OF MOTOR AND PUMP

The design of the system starts with the motor rating. Based on the load requirement, the motor is designed as follows [28]:

$$Waterpower(kW) = \frac{9.81 \times Q(L/s) \times H(m) \times \rho}{1000} \quad (1)$$

$$Motorpower(kW) = \frac{Waterpower(kW)}{\eta_p \times \eta_d} \quad (2)$$

where H is the total head, Q is the flow discharge and ρ is the specific gravity of water. η_p, η_d represents the efficiency of the pump and motor drive, respectively. A motor rating of 745 W is considered for simulation. Based on the motor rating, the pump constant is determined using affinity laws as follows [28]:

$$K_{pump} = \frac{T_L}{\omega^2} \quad (3)$$

where T_L and ω represents the load torque and speed of the motor in (N-m) and (rad/sec), respectively.

B. DESIGN OF PV ARRAY

For the induction motor 745 W an 900 W_p PV array is chosen. A 100 W_p panel is considered for (3 × 3) PV array. The TCT array current is determined as follows [29]:

$$I_{ij(shaded)} = KI_{ij(standard)} \quad (4)$$

where

$$K = \frac{G_{ij}}{G_{STC}} \quad (5)$$

where i, j represents the row and column of an array. $I_{ij(shaded)}$ and $I_{ij(standard)}$ represents the module current, during shaded and standard irradiance (1000 W/m^2). G_{ij} represents the irradiance received by the ij module and G_{STC} represents standard irradiance. The PV array voltage is determined as follows [29]:

$$V_{pv} = \sum_{i=1}^{m} V_i \quad (6)$$

TABLE 1. PV module specifications.

Parameters	Value
Maximum Power (P_{mp})	100 W_p
Open Circuit Voltage (V_{oc})	147 V
Short Circuit Current (I_{sc})	0.84 A
Voltage at MPP (V_{mp})	125 V
Current at MPP (I_{mp})	0.8 A

where m indicates the total number of rows, i indicates the row number, V_i is the voltage of the i^{th} row and V_{pv} represents the array voltage. Table 1 represents the specifications of the PV module.

C. DESIGN OF IRRADIANCE SENSORS AND SWITCHES FOR DR ALGORITHM

Sensors and switches play a crucial role in DR. The number of switches and sensors depends on the number of modules, number of rows, and columns in TCT configuration. The switches requirement are given by the following equation [29]:

$$S_{SPST} = 2 \times m^2 \times n \tag{7}$$

where S_{SPST} represents the number of single pole single throw switches, m and n represent the number of rows and columns in a TCT PV array. The number of sensors required is given as follows:

$$I_s = N \tag{8}$$

where I_s, N represents the number of irradiance sensors and the PV modules, respectively.

D. DESIGN OF CONVERTERS

The design of the inductance and capacitance of the boost converter plays a vital role in deciding the system's performance. The inductance (L) and capacitance (C_{PV}) are derived from the following equations [23], [30]:

$$L = \frac{V_{PV}^2}{0.1 \times P_{PV} \times f_s}\left(1 - \frac{V_{PV}}{V_{dc}}\right) \tag{9}$$

$$C_{pv} = \frac{(\Delta I_{pv})}{(8 \times \Delta V_{pv} \times f_s)} \tag{10}$$

where, V_{dc}, V_{PV}, I_{PV}, P_{PV} and f_s represents dc-link and array voltage, PV array current, power and switching frequency. For $V_{dc} = 400$ V, the duty cycle for the boost converter is $D = 0.0625$. The switching frequency of the converter and $\Delta V_{dc}/V_{dc}$ is chosen as 10 kHz and 0.0001, respectively. The inductance and capacitance values are determined as 9.76 mH, 64 μF and are chosen as 10 mH, 65 μF, respectively. The design of dc-link voltage depends on the pulse width modulation technique used for the inverter. The relation between dc-link voltage and the line voltage of motor for the sinusoidal pulse width modulation (SPWM) technique is as follows [25]:

$$v_{LL} = 0.612 \times m_a \times v_{dc} \tag{11}$$

TABLE 2. Design considerations of the proposed system.

Parameters	Value
I_s	9
S_{SPST}	54
L	10 mH
C_{PV}	65 μF
C_{dc}	1050 μF
K_{pump}	$2.22149e^{-4} N.m/(rad/sec)^2$

where v_{LL} is the line voltage of the motor. For 230 V line voltage V_{dc} is calculated as 375 V. It is chosen as 400 V for simulation. The dc-link capacitance (C_{dc}) is determined as follows [8]:

$$C_{dc} = \frac{6\alpha VIt}{V_{dc}^{*2} - V_{dc_1}^2} \tag{12}$$

where, V_{dc}^* refers to the reference dc bus voltage, while V_{dc_1} is acceptable to the lowermost voltage during transients and is chosen as 375 V, α is overloading factor (1.2), V and I are the motor phase voltage and current, t is transient duration. The C_{dc} is estimated as 1025 μF and is chosen as 1050 μF. The overall design considerations are tabulated in Table 2.

III. PROPOSED SYSTEM CONTROL

The proposed control strategy initially uses sensors and switches to enhance the power output in the TCT PV array. The MPPT algorithm helps to operate the load at maximum power. The PI controller regulates the dc-link voltage, and V/f control is used to drive the induction motor.

Fig. 2 shows the flowchart of the proposed dynamic reconfiguration algorithm. During partial shading, various modules in the TCT array receive different irradiances. These different irradiances result in varying currents in rows of the TCT PV array. Due to the difference in row currents, the TCT array exhibits multiple peaks [29]. Since in TCT, the panels in one row are connected in parallel and several such rows are connected in series, the lowest current among the rows will be the output current. This lowest current minimizes the output power of the TCT PV array. So the proposed algorithm aims at equalizing the current in rows to enhance output power from the TCT PV array.

The proposed DR triggers the switches based on the proposed algorithm. The algorithm uses the irradiance sensor data of each module to alter the connections. Let G and P indicate the irradiances and their corresponding position of modules in a PV array ($m \times n$).

$$G = \begin{bmatrix} G_{11} & G_{12} & G_{13} \\ G_{21} & G_{22} & G_{23} \\ G_{31} & G_{32} & G_{33} \end{bmatrix} \tag{13}$$

$$P = \begin{bmatrix} P_{11} & P_{12} & P_{13} \\ P_{21} & P_{22} & P_{23} \\ P_{31} & P_{32} & P_{33} \end{bmatrix} \tag{14}$$

Let Z corresponds to the row-wise summation of the G matrix.

$$Z = \begin{bmatrix} Z_{11} \\ Z_{21} \\ Z_{31} \end{bmatrix} \tag{15}$$

The algorithm computes the set value based on the irradiances as given below

$$Setvalue = \frac{\sum_{i=1,j=1}^{i=m,j=n} G_{i,j}}{m} \tag{16}$$

where i, j represents corresponding module positions and m, n represents number of rows and columns.

For simplifying the irradiance equalization process, the algorithm initially sorts the elements of G and the corresponding P matrix in column-wise order. Based on the sorted G matrix, the Z matrix is determined. The algorithm determines whether each element in Z is equal to the set value. If all the elements in Z are not equal to the set value, then the algorithm determines the rows of G in which the elements need to exchange. The switch matrix control is based on row selection. The algorithm determines the row index corresponding to the minimum and maximum element in Z and stores it in *Min_pos* and *Max_pos*. Some of the G matrix elements corresponding to *Min_pos* and *Max_pos* rows need to be swapped to make all the values in the Z matrix near to the set value.

Let u, and v indicate the position of irradiances in rows of G matrix corresponding to *Max_pos* and *Min_pos*. The elements to be swapped in the G matrix are selected so that the difference between those elements in *Min_pos* and *Max_pos* rows is nearer to the difference between a maximum element in Z and the set value.

If all the Z matrix elements are not equal to the set value, then the algorithm will be repeated. If the elements swapped in the previous iteration are again getting swapped in the present iteration, the algorithm terminates. Finally, based on the module positions, the corresponding switches are triggered to generate enhanced power during the partial shading conditions. The output of PV power has enhanced; however, it is necessary to operate the load at maximum power. A conventional incremental conductance algorithm is used for MPPT operation.

Once the MPPT is reached, the inverter dc-link voltage should be maintained constant for the effective operation of the motor. The PI controller regulates the dc-link voltage as follows:

$$V_{errorDC(n)} = V_{dc}^{*} - V_{dc} \tag{17}$$

where V_{dc}^{*} represents the reference value and V_{dc} represents the output of the boost converter. The output of the proportional–integral (PI) controller generates a speed, as represented in the below equation [8].

$$\omega_1(n) = \omega_1(n-1) + K_p(V_{dc}(n) - V_{dc}(n-1)) + K_i V_{dc}(n) \tag{18}$$

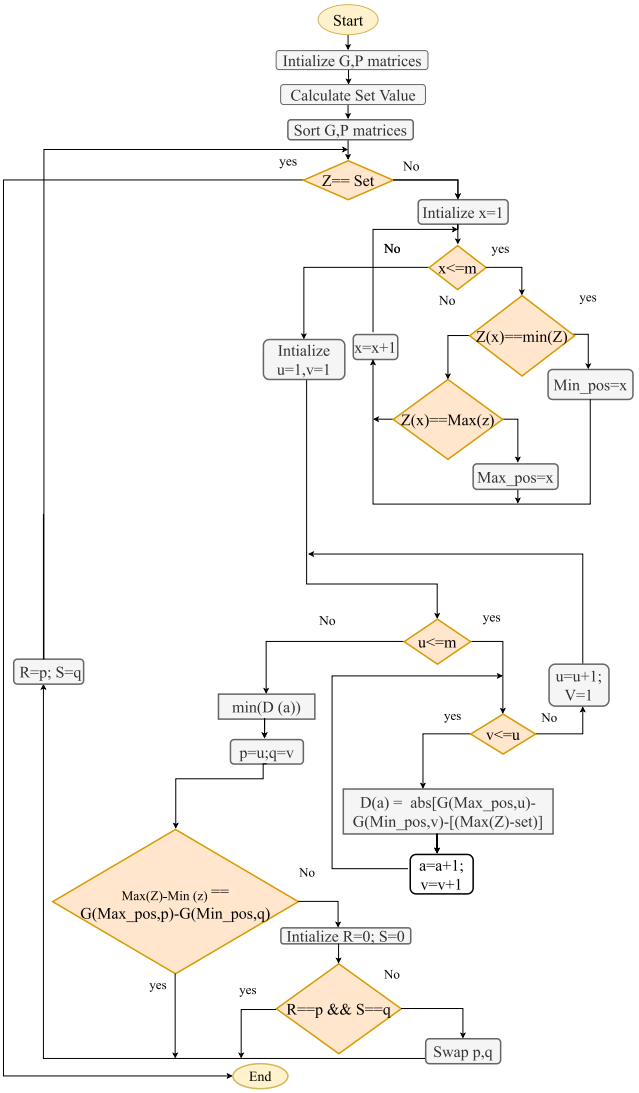

FIGURE 2. Flowchart for the proposed reconfiguration algorithm.

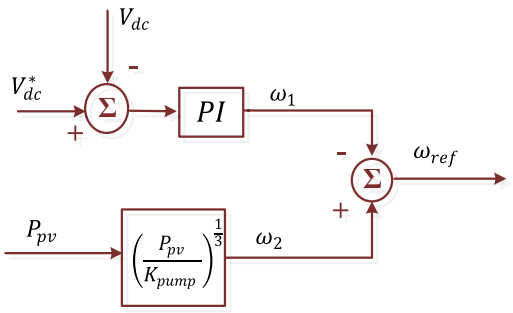

FIGURE 3. Block diagram for the generation of reference speed.

The reference speed for V/f is obtained from the pump affinity and the output of the PI controller, as shown in Fig. 3. The integration of ω generates θ, which is used to obtain the sinusoidal voltages as shown in Fig. 4. By controlling the frequency, the modulation index changes. The sinusoidal

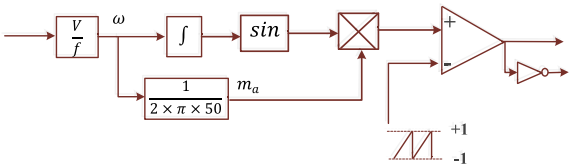

FIGURE 4. Block diagram for gate pulse generation.

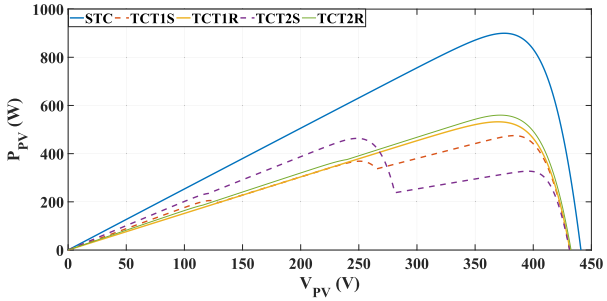

FIGURE 5. $P-V$ curves of case-1 under STC, shading and reconfiguration.

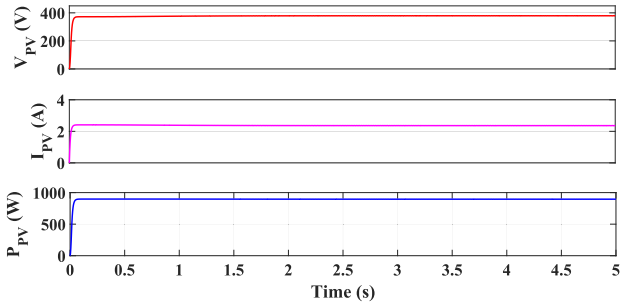

FIGURE 6. Source side performance of the BIPVPS under STC.

voltages are compared with a high-frequency triangular wave to generate pulses for the inverter to control the speed of the motor.

Therefore, the study forms a complete framework for the successful operation of the PV-fed motor under partial shading conditions.

IV. RESULTS AND ANALYSIS

A. SIMULATION RESULT ANALYSIS

During standard test conditions (STC), the TCT array generates a power of 900 W_p, as shown in Fig. 5.

Two shading patterns are considered to show the efficiency of the proposed SPWPS. In TCT1S, irradiance levels seen by each module is as follows:

$$\text{TCT1S} = \begin{bmatrix} 400 & 500 & 600 \\ 500 & 600 & 700 \\ 600 & 700 & 800 \end{bmatrix} \tag{19}$$

The row current corresponding to TCT1S pattern is given as follows:

$$I_{R1} = ((\frac{400}{1000}) + (\frac{500}{1000}) + (\frac{600}{1000})) \times I_m = 1.5 \times I_m \tag{20}$$

$$I_{R2} = ((\frac{500}{1000}) + (\frac{600}{1000}) + (\frac{700}{1000})) \times I_m = 1.8 \times I_m \tag{21}$$

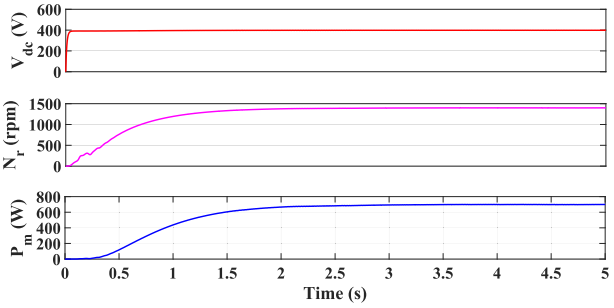

FIGURE 7. Load side performance of the BIPVPS under STC.

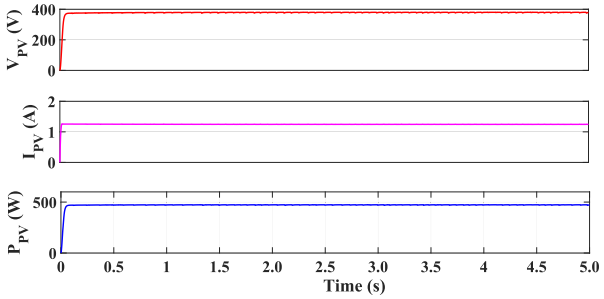

FIGURE 8. Source side performance of the BIPVPS under TCT1S.

$$I_{R3} = ((\frac{600}{1000}) + (\frac{700}{1000}) + (\frac{800}{1000})) \times I_m = 2.1 \times I_m \tag{22}$$

From the above equations, three different peaks occur in the $P-V$ curve, as evident from the above equations with three different row currents. The governing equations of current after reconfiguration is given as follows:

$$I_{R1} = ((\frac{500}{1000}) + (\frac{600}{1000}) + (\frac{700}{1000})) \times I_m = 1.8 \times I_m \tag{23}$$

$$I_{R2} = ((\frac{500}{1000}) + (\frac{600}{1000}) + (\frac{700}{1000})) \times I_m = 1.8 \times I_m \tag{24}$$

$$I_{R3} = ((\frac{400}{1000}) + (\frac{600}{1000}) + (\frac{800}{1000})) \times I_m = 1.8 \times I_m \tag{25}$$

After reconfiguration according to the proposed algorithm, the module position changes. After reconfiguration, all the row currents are equal, which enables a single peak $P-V$ curve, as shown in Fig. 5.

Fig. 6 & 7 shows the source and load side performance during STC. Fig. 8 shows the source side performance under TCT1S. The maximum PV array power is 472 W for TCT1S. Based on the available input PV power, the motor rotates at a speed and torque of 1104 rpm and 3.7 N-m, respectively. The dc-link voltage and motor speed for TCT1S is shown in Fig. 9.

After reconfiguration, since the I_{PV} increases and the mismatch losses decreases, the overall PV array power increase, as shown in Fig. 10. The PV power after reconfiguration is 523 W. The input power increases by 10.8 % compared to TCT1S. The dc- link voltage remains at 400 V. The ratio of V/f remains constant in TCT1S and TCT1R, as shown in Table 3. Since the PV power enhances, the power delivered to the motor increases, which aids in increasing the motor speed.

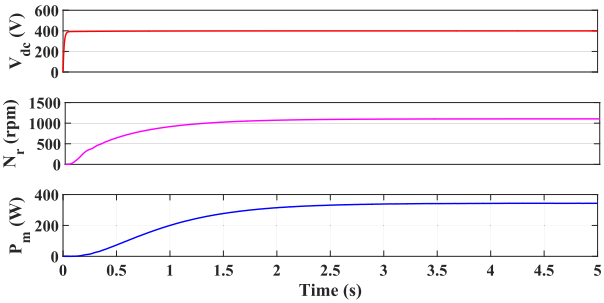

FIGURE 9. Load side performance of the BIPVPS under TCT1S.

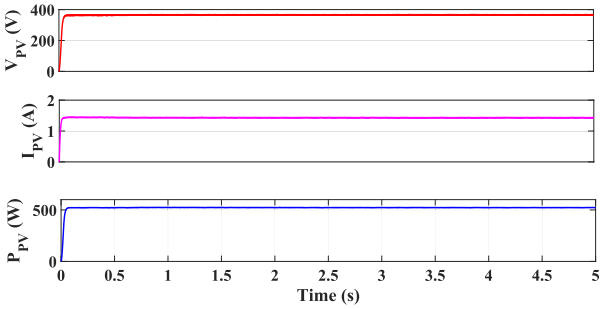

FIGURE 10. Source side performance of the BIPVPS under TCT1R.

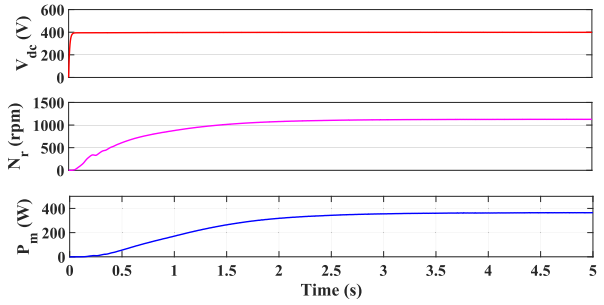

FIGURE 11. Load side performance of the BIPVPS under TCT1R.

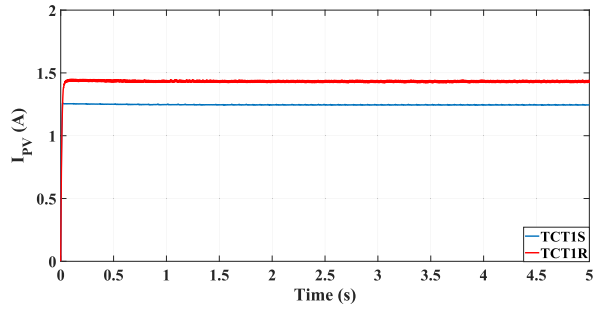

FIGURE 12. Comparison of PV array current during TCT1S and TCT1R.

Fig. 11 shows the corresponding dc-link voltage, speed and motor power for TCT1R. Fig. 12 & 13 show the comparison of PV current, power during TCT1S and TCT1R. The PV current and power were enhanced after reconfiguration. Therefore under this shading condition, the system performances enhanced with the same available source.

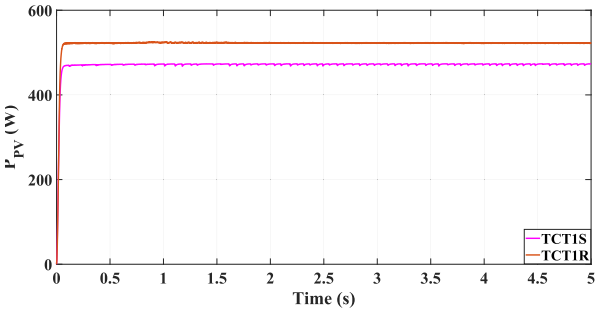

FIGURE 13. Comparison of PV array power during TCT1S and TCT1R.

The second shading is considered such a way that one of the rows of the TCT receives very low irradiances compared to the other two rows. During such conditions, the global peak will be far away from the open-circuit voltage and it always occurs on the left side of the P-V curve. The following irradiance profile is chosen for TCT2S shading:

$$\text{TCT2S} = \begin{bmatrix} 800 & 700 & 900 \\ 800 & 600 & 900 \\ 300 & 350 & 350 \end{bmatrix} \tag{26}$$

The row currents corresponding to TCT2S are represented in (27)-(29), respectively. The TCT2S is considered to show the performance of the BIPVPS works effectively with the conventional MPPT algorithm.

$$I_{R1} = ((\frac{800}{1000}) + (\frac{700}{1000}) + (\frac{900}{1000})) \times I_m = 2.4 \times I_m \tag{27}$$

$$I_{R2} = ((\frac{800}{1000}) + (\frac{600}{1000}) + (\frac{900}{1000})) \times I_m = 2.3 \times I_m \tag{28}$$

$$I_{R3} = ((\frac{300}{1000}) + (\frac{350}{1000}) + (\frac{350}{1000})) \times I_m = 1.0 \times I_m \tag{29}$$

During this case, three different row currents appear; as a result, three distant peaks occur in the $P-V$ curve. After reconfiguration, the difference between the row currents is small. Therefore, it appears as a single peak, as shown in Fig. 5. After reconfiguration, the row currents are represented in (30)-(32), respectively.

$$I_{R1} = ((\frac{300}{1000}) + (\frac{800}{1000}) + (\frac{800}{1000})) \times I_m = 1.9 \times I_m \tag{30}$$

$$I_{R2} = ((\frac{350}{1000}) + (\frac{600}{1000}) + (\frac{900}{1000})) \times I_m = 1.85 \times I_m \tag{31}$$

$$I_{R3} = ((\frac{350}{1000}) + (\frac{700}{1000}) + (\frac{900}{1000})) \times I_m = 1.95 \times I_m \tag{32}$$

The row current equations after reconfiguration reveal that the mismatch losses will reduce, which will enhance the PV power. The P_{PV} during TCT2S shading is 318 W, as shown in Fig. 14. Although the global power is 463 W, the BIPVPS with conventional MPPT tracks 318 W. Since the local peak exists on the right side of the $P-V$ curve, which is shown in Fig. 5. Therefore, the speed of the motor is 938 rpm, which is relatively low compared to the other cases, as shown in Fig. 15.

TABLE 3. Performance comparison of water pumping system under standard, partial shading and reconfiguration conditions.

S.no	Cases	V_{PV} (V)	I_{PV} (A)	P_{PV} (W)	m_a	f (Hz)	Speed (rpm)	Torque (N-m)
1	STC	379.2	2.36	896	0.94	47.13	1398	6.09
2	TCT1S	379	1.24	472	0.73	37.29	1104	3.7
3	TCT1R	365	1.43	523	0.75	37.6	1126	4
4	TCT2S	379	0.84	318	0.63	31.5	938	2.8
5	TCT2R	382	1.44	552	0.78	39.01	1161	4.15

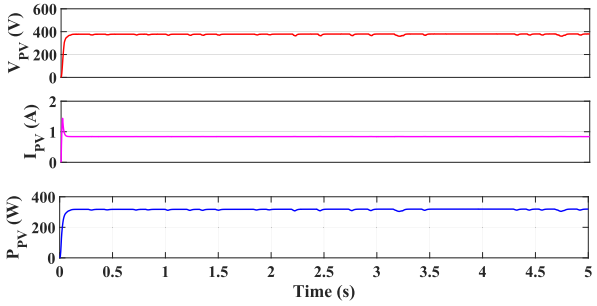

FIGURE 14. Source side performance of the BIPVPS under TCT2S.

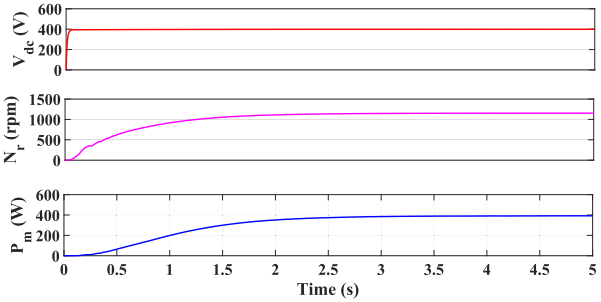

FIGURE 17. Load side performance of the BIPVPS under TCT2R.

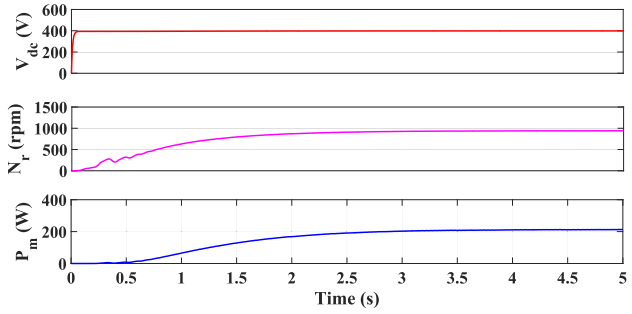

FIGURE 15. Load side performance of the BIPVPS under TCT2S.

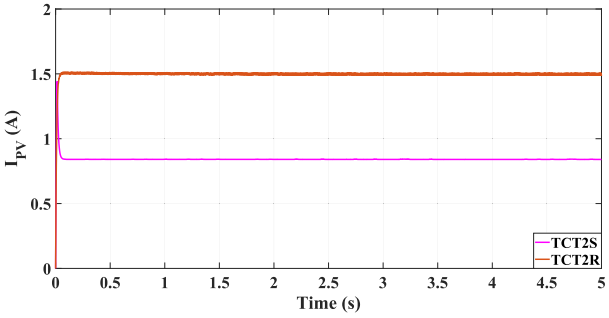

FIGURE 18. Comparison of PV array current during TCT2S and TCT2R.

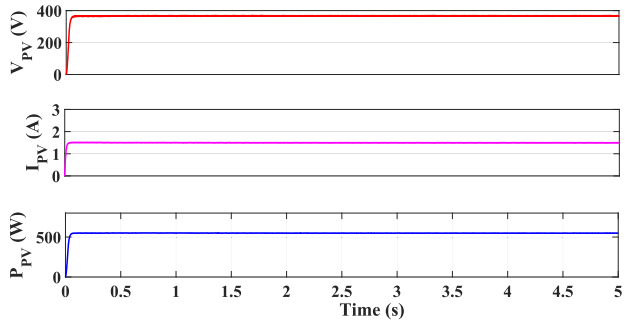

FIGURE 16. Source side performance of the BIPVPS under TCT2R.

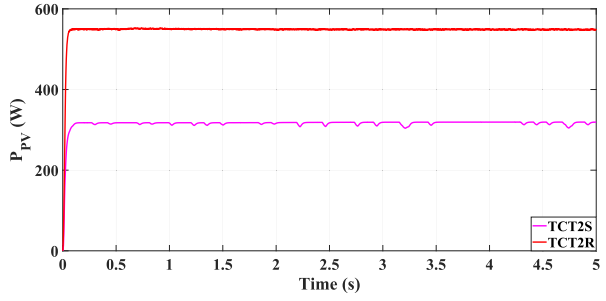

FIGURE 19. Comparison of PV array power during TCT2S and TCT2R.

After reconfiguration, the PV array power is 552 W, as shown in Fig. 16. Thus the PV power has been enhanced to 73.58% compared to the TCT2S. The PV array current and power before and after reconfiguration are shown in Fig. 18 & 19, respectively. The speed is enhanced to 23.7%, compared to the TCT2S. The performance comparison of the proposed system under different shading conditions, shown in Table 3.

During TCT2R, the reference frequency value is 39 Hz, and the modulation index is 0.78, demonstrating that the ratio of V/f is maintained constant. Moreover, the dc-link voltage is settled to a reference value of 400 V during all the shading and reconfiguration conditions which resemble the effectiveness of PI controller operation. The PI controller is tuned using a closed-loop PI auto tuner using Matlab. In both the shading cases, the proposed algorithm enhances the output power whether the maximum power is either nearer or far away from the open-circuit voltage. After reconfiguration, the

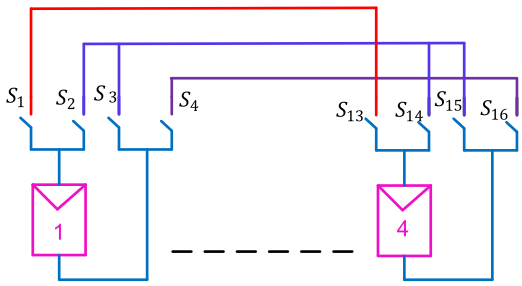

FIGURE 20. Switch network.

maximum power is nearer to open-circuit voltage, enabling conventional MPPT with the proposed algorithm.

B. EXPERIMENTAL RESULTS ANALYSIS

The proposed dynamic reconfiguration algorithm is initially implemented on a (2 × 2) TCT PV array for validation. The switching logic circuit for a PV module is shown in Fig. 20. The switches S_1, S_2, S_3, and S_4 are used to alter the position of module-1 in row-1 & 2. Similarly, switches (S_5, S_6, S_7, S_8), (S_9, S_{10}, S_{11}, S_{12}) and (S_{13}, S_{14}, S_{15}, S_{16}) are used to alter the position of modules-2, 3 and 4 in row-1 & 2 respectively. Initially at t = 0 s, the modules of (2 × 2) TCT PV array are subjected to the following irradiance:

$$G = \begin{bmatrix} 400 & 500 \\ 500 & 600 \end{bmatrix}$$

At t = 2.5 s the irradiance profile is changed as follows:

$$G = \begin{bmatrix} 400 & 400 \\ 600 & 600 \end{bmatrix}$$

The working of the DR algorithm is visualized by the switching logic of the switches (S_9-S_{16}) as shown in Fig. 21 & 22 respectively. During the initial shading pattern at t = 0 s, the switches S_{10} and S_{12} are switched on, which indicates that module-3 will remain in the same position (second row) as TCT configuration. The switches S_{13} and S_{15} are turned on, which alter the position of module-4 to the first row as its initial position is the second row in TCT configuration. Similarly, module-2 switches S_6 and S_8 are turned on to change the position of the module to the second row.

At t = 2.5 s, the switches S_9 and S_{11} are turned on, which indicates module-3 will alter the position to the first row. The switches S_{14} and S_{16} are switched on to remain module-4 in the first row. Similarly, the switches of modules-1&2 correspondingly turned on to make the irradiance equalization in rows to enhance the output power. The algorithm is applicable to any size PV array. However, the system is more reliable for smaller size PV array. For simplicity the P-V characteristics before and after reconfiguration are emulated using PV simulator (Chroma 62050H-600S programmable DC power supply). The prototype for experimental verification is shown in Fig. 23. The PV module specifications used

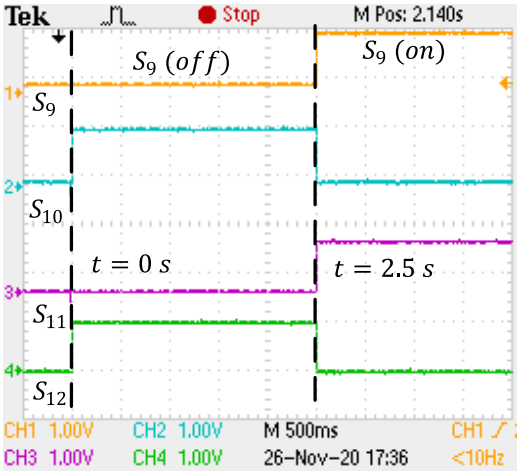

FIGURE 21. Variation of switches S_9 - S_{12} during change in irradiance.

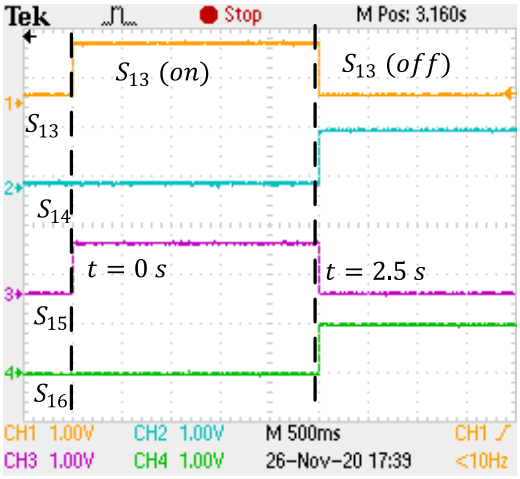

FIGURE 22. Variation of switches S_{13} - S_{16} during change in irradiance.

are $V_{oc} = 98\ V$, $I_{sc} = 0.52\ A$, $V_{mp} = 83.3\ V$ and $I_{mp} = 0.5\ A$. A 745 W three-phase induction motor 415 V, 1.9 A, 1405 rpm is used for implementation. The dc-link voltage is selected as 300 V. The pump characteristics are realized using a DC generator with a resistive load box.

A hall effect sensors are used for voltage and current measurement. The gating pulses for the converter are fed through a DSP processor.

Fig. 24 shows the PV side performance during STC. The scaling factor for current and power is (k = 0.5), since two turns are used for the measurement of current. The indices $V_{PV} = 250$ V, $I_{PV} = 1.5$ A and $P_{PV} = 375$ W indicates the effectiveness of MPPT operation. The $V_{dc} = 300$ V demonstrates PI controller operation.

Fig. 25 & 26 shows the PV side performance under TCT1S and TCT1R, respectively. It is observed that the V_{dc} and P_{PV} are 300 V and 196 W for TCT1S. After reconfiguration, the P_{PV} power increases by 24 W. Since the PV power enhances, the speed of the induction motor also increases.

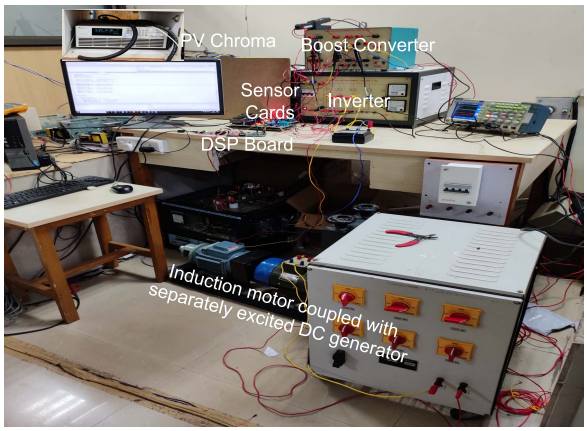

FIGURE 23. Experimental prototype.

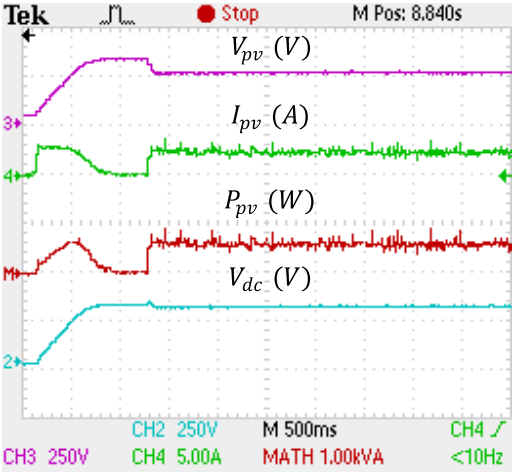

FIGURE 24. PV side performance of the BIPVPS under STC.

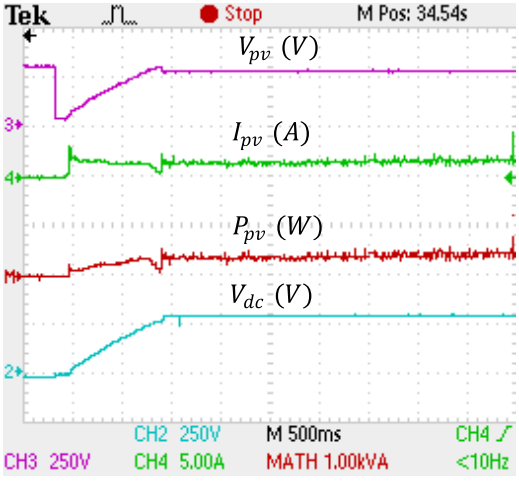

FIGURE 25. PV side performance of the BIPVPS under TCT1S.

Fig. 27 shows the MPPT performance during TCT2S and TCT2R. It is observed that the MPPT tracks the local maximum in the $I-V$ curve during TCT2S, as shown in Fig. 27 (a).

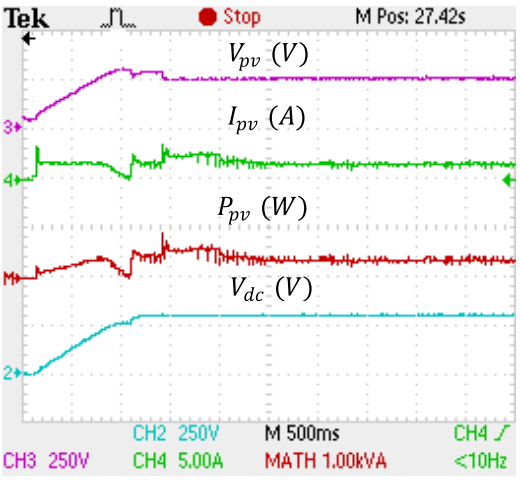

FIGURE 26. PV side performance of the BIPVPS under TCT1R.

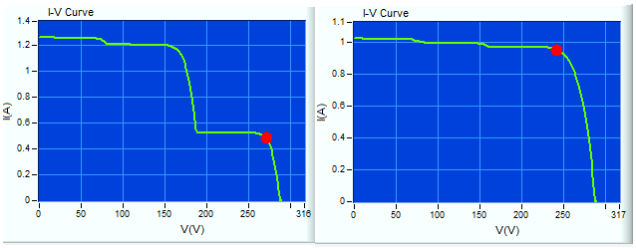

(a) (b)

FIGURE 27. MPPT performance for TCT2S and TCT2R using PV-chroma.

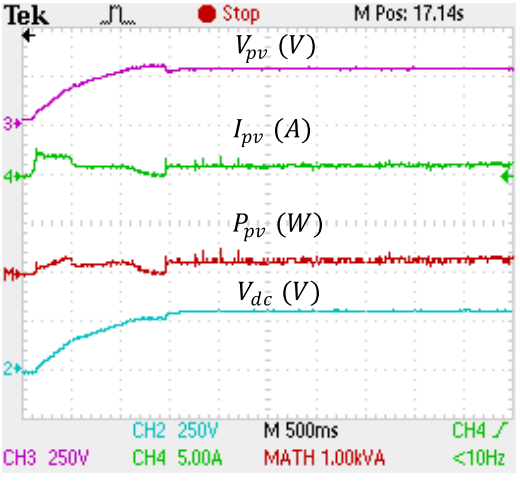

FIGURE 28. PV side performance of the BIPVPS under TCT2S.

As the MPPT tracks the local peak, the P_{PV} is significantly less (i.e., 135 W), as shown in Fig. 28. However, after reconfiguration, the MPPT algorithm tracks the global peak, as shown in Fig. 27 (b). Therefore, the P_{PV} is 225 W, as shown in Fig. 29, which allows the motor to run faster compared to the shading condition. Therefore, the proposed system can deliver more amount of water. Although the proposed system requires sensors and switches for reconfiguration, it is

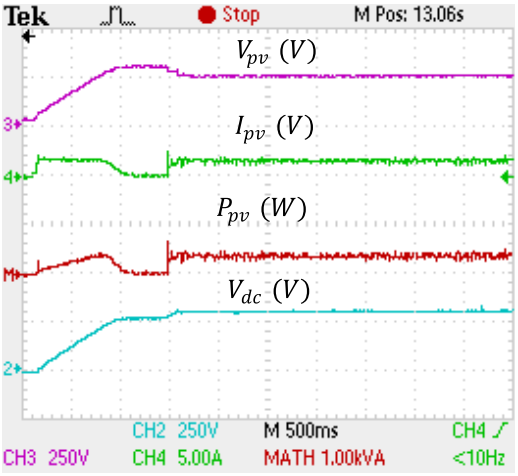

FIGURE 29. PV side performance of the BIPVPS under TCT2R.

a one-time arrangement, which significantly enhances the output power of the PV array. The proposed method effectively utilizes the PV array source and improves the system reliability and efficiency.

V. CONCLUSION

This paper introduces a novel dynamic array reconfiguration to enhance the performance of BIPVPS under partial shading conditions. The proposed reconfiguration scheme using switches and sensors enhances the TCT array output power. During TCT2R condition, the PV power has been enhanced to 73.5% compared to TCT2S. As the PV power increases, it enhances the torque and speed of the induction motor. Further, during all the shading and reconfiguration conditions, the V/f remains constant, which helps in the smooth operation of the induction motor. During most shading conditions, the global peak with proposed reconfiguration appeared on the right side of the P-V curve eliminating the necessity of complex MPPT techniques. Thus the proposed system is simple and efficient.

REFERENCES

[1] C. Peng, Y. Huang, and Z. Wu, "Building-integrated photovoltaics (BIPV) in architectural design in China," *Energy Buildings*, vol. 43, no. 12, pp. 3592–3598, Dec. 2011.
[2] V. C. Sontake and V. R. Kalamkar, "Solar photovoltaic water pumping system—A comprehensive review," *Renew. Sustain. Energy Rev.*, vol. 59, pp. 1038–1067, Jun. 2016.
[3] S. Angadi, U. R. Yaragatti, Y. Suresh, and A. B. Raju, "Comprehensive review on solar, wind and hybrid wind-PV water pumping systems—An electrical engineering perspective," *CPSS Trans. Power Electron. Appl.*, vol. 6, no. 1, pp. 1–19, Mar. 2021.
[4] H. Patel and V. Agarwal, "MATLAB-based modeling to study the effects of partial shading on PV array characteristics," *IEEE Trans. Energy Convers.*, vol. 23, no. 1, pp. 302–310, Mar. 2008.
[5] A. Mäki and S. Valkealahti, "Effect of photovoltaic generator components on the number of MPPs under partial shading conditions," *IEEE Trans. Energy Convers.*, vol. 28, no. 4, pp. 1008–1017, Dec. 2013.
[6] R. B. Bollipo, S. Mikkili, and P. K. Bonthagorla, "Hybrid, optimal, intelligent and classical PV MPPT techniques: A review," *CSEE J. Power Energy Syst.*, vol. 7, no. 1, pp. 9–33, Jan. 2021.
[7] D. P. Winston, S. Kumaravel, B. P. Kumar, and S. Devakirubakaran, "Performance improvement of solar PV array topologies during various partial shading conditions," *Sol. Energy*, vol. 196, pp. 228–242, Jan. 2020.
[8] B. Singh, U. Sharma, and S. Kumar, "Standalone photovoltaic water pumping system using induction motor drive with reduced sensors," *IEEE Trans. Ind. Appl.*, vol. 54, no. 4, pp. 3645–3655, Jul. 2018.
[9] S. Sashidhar and B. G. Fernandes, "A novel ferrite SMDS spoke-type BLDC motor for PV bore-well submersible water pumps," *IEEE Trans. Ind. Electron.*, vol. 64, no. 1, pp. 104–114, Jan. 2017.
[10] N. D. Kaushika and N. K. Gautam, "Energy yield simulations of interconnected solar PV arrays," *IEEE Trans. Energy Convers.*, vol. 18, no. 1, pp. 127–134, Mar. 2003.
[11] S. R. Pendem, S. Mikkili, and P. K. Bonthagorla, "PV distributed-MPP tracking: Total-cross-tied configuration of string-integrated-converters to extract the maximum power under various PSCs," *IEEE Syst. J.*, vol. 14, no. 1, pp. 1046–1057, Mar. 2020.
[12] G. Sai Krishna and T. Moger, "Reconfiguration strategies for reducing partial shading effects in photovoltaic arrays: State of the art," *Sol. Energy*, vol. 182, pp. 429–452, Apr. 2019.
[13] D. Nguyen and B. Lehman, "A reconfigurable solar photovoltaic array under shadow conditions," in *Proc. 23rd Annu. IEEE Appl. Power Electron. Conf. Expo.*, Feb. 2008, pp. 980–986.
[14] M. Manjunath, B. V. Reddy, and B. Lehman, "Performance improvement of dynamic PV array under partial shade conditions using M2 algorithm," *IET Renew. Power Gener.*, vol. 13, no. 8, pp. 1239–1249, Jun. 2019.
[15] M. Kolhe, J. C. Joshi, and D. P. Kothari, "Performance analysis of a directly coupled photovoltaic water-pumping system," *IEEE Trans. Energy Convers.*, vol. 19, no. 3, pp. 613–618, Sep. 2004.
[16] R. Kumar and B. Singh, "BLDC motor-driven solar PV array-fed water pumping system employing zeta converter," *IEEE Trans. Ind. Appl.*, vol. 52, no. 3, pp. 2315–2322, May 2016.
[17] R. Kumar and B. Singh, "Solar PV powered-sensorless BLDC motor driven water pump," *IET Renew. Power Gener.*, vol. 13, no. 3, pp. 389–398, Feb. 2019.
[18] R. Kumar and B. Singh, "Solar PV powered BLDC motor drive for water pumping using Cuk converter," *IET Elect. Power Appl.*, vol. 11, no. 2, pp. 222–232, Feb. 2017.
[19] S. Sashidhar, V. Guru Prasad Reddy, and B. G. Fernandes, "A single-stage sensorless control of a PV-based bore-well submersible BLDC motor," *IEEE J. Emerg. Sel. Topics Power Electron.*, vol. 7, no. 2, pp. 1173–1180, Jun. 2019.
[20] S. Jain, R. Karampuri, and V. T. Somasekhar, "An integrated control algorithm for a single-stage PV pumping system using an open-end winding induction motor," *IEEE Trans. Ind. Electron.*, vol. 63, no. 2, pp. 956–965, Feb. 2016.
[21] S. Jain, A. K. Thopukara, R. Karampuri, and V. T. Somasekhar, "A single-stage photovoltaic system for a dual-inverter-fed open-end winding induction motor drive for pumping applications," *IEEE Trans. Power Electron.*, vol. 30, no. 9, pp. 4809–4818, Sep. 2015.
[22] M. A. Vitorino, M. B. de Rossiter Correa, C. B. Jacobina, and A. M. N. Lima, "An effective induction motor control for photovoltaic pumping," *IEEE Trans. Ind. Electron.*, vol. 58, no. 4, pp. 1162–1170, Apr. 2011.
[23] A. Mudlapur, V. V. Ramana, R. V. Damodaran, V. Balasubramanian, and S. Mishra, "Effect of partial shading on PV fed induction motor water pumping systems," *IEEE Trans. Energy Convers.*, vol. 34, no. 1, pp. 530–539, Mar. 2019.
[24] M. Matam, V. R. Barry, and A. R. Govind, "Optimized reconfigurable PV array based photovoltaic water-pumping system," *Sol. Energy*, vol. 170, pp. 1063–1073, Aug. 2018.
[25] K. Khan, S. Shukla, and B. Singh, "Performance-based design of induction motor drive for single-stage PV array fed water pumping," *IEEE Trans. Ind. Appl.*, vol. 55, no. 4, pp. 4286–4297, Jul. 2019.
[26] H. J. Lee, S. H. Im, D. Y. Um, and G. S. Park, "A design of rotor bar for improving starting torque by analyzing rotor resistance and reactance in squirrel cage induction motor," *IEEE Trans. Magn.*, vol. 54, no. 3, pp. 1–4, Mar. 2018.
[27] E. Drury, T. Jenkin, D. Jordan, and R. Margolis, "Photovoltaic investment risk and uncertainty for residential customers," *IEEE J. Photovolt.*, vol. 4, no. 1, pp. 278–284, Jan. 2014.
[28] M. N. Ibrahim, H. Rezk, M. Al-Dhaifallah, and P. Sergeant, "Solar array fed synchronous reluctance motor driven water pump: An improved performance under partial shading conditions," *IEEE Access*, vol. 7, pp. 77100–77115, 2019.

[29] J. P. Storey, P. R. Wilson, and D. Bagnall, "Improved optimization strategy for irradiance equalization in dynamic photovoltaic arrays," *IEEE Trans. Power Electron.*, vol. 28, no. 6, pp. 2946–2956, Jun. 2013.
[30] R. K. Jain, V. R. Barry, and G. H. K. Varma, "Model based design and sliding mode control approach for two stage water pumping system with reduced sensors," *IEEE J. Emerg. Sel. Topics Power Electron.*, early access, Jul. 27, 2021, doi: 10.1109/JESTPE.2021.3100477.
[31] A. Tomar, P. H. Nguyen, and S. Mishra, "SEPIC-MISO converter based PV water pumping System- an improved performance under mismatching conditions," in *Proc. IEEE 9th Power India Int. Conf. (PIICON)*, Feb. 2020, pp. 1–5.
[32] H. K. V. Gadiraju, B. V. Reddy, and R. K. Jain, "Reconfiguration based single stage PV water pumping system," in *Proc. Nat. Power Electron. Conf. (NPEC)*, Dec. 2019, pp. 1–4.
[33] S. Kumar and B. Singh, "Performance of MPPT and effect of partial shading on PV array fed LEV with sensorless control," in *Proc. IEEE 4th Int. Conf. Comput., Power Commun. Technol. (GUCON)*, Sep. 2021, pp. 1–7.

GADIRAJU HARISH KUMAR VARMA (Graduate Student Member, IEEE) was born in Andhra Pradesh, India, in 1992. He received the B.Tech. degree in electrical and electronics engineering from the SRKR Engineering College, Bhimavaram, India, in 2013, and the M.Tech. degree in power electronic drives from the Gudlavalleru Engineering College, Gudlavalleru, India, in 2015. He is currently pursuing the Ph.D. degree in electrical engineering with the Department of Electrical and Electronics Engineering, National Institute of Technology Goa, India. His research interests include renewable energy applications, PV array reconfigurations, and multilevel inverters.

VENUGOPAL REDDY BARRY (Member, IEEE) received the B.Tech. degree in electrical engineering from the JNTU College of Engineering, Hyderabad, India, in 2001, and the M.Tech. and Ph.D. degrees from the National Institute of Technology, Warangal, India, in 2005 and 2013, respectively. He is currently working as an Associate Professor with the Department of Electrical Engineering, National Institute of Technology, Goa, India. His research interests include renewable energy systems, PV array reconfigurations, multilevel inverters, multilevel PWM switching strategies, and multilevel inversion realized through open-end winding Induction motor drives.

ROHIT KUMAR JAIN was born in Bundi, Rajasthan, India, in 1994. He received the B.Tech. degree (Hons.) in electrical engineering from the University College of Engineering, Rajasthan Technical University, Kota, India, in 2016, and the M.Tech. degree in power electronics and power system from the National Institute of Technology, Goa, India, in 2019, where he is currently pursuing the Ph.D. degree with the Department of Electrical and Electronics Engineering. His current research interests include design and development of control of power electronic converter, inverter and power electronic drives for renewable sources for water pumping application, and grid connected systems.